

# Effects of Spectral UV on Degradation of Acrylic-Urethane Coatings

by

**Tinh Nguyen, Jonathan W. Martin, Eric Byrd and Edward Embree**  
**Building and Fire Research Laboratory**  
**National Institute of Standards and Technology**  
**Gaithersburg, MD 20899 USA**

**Reprinted from the Proceedings of the 80th Annual Meeting of the Program of the FSCT, Federation of Societies for Coatings Technology, October 30-November 1, 2002, New Orleans, LA, CD-ROM, 2002.**

**NOTE: This paper is a contribution of the National Institute of Standards and Technology and is not subject to copyright.**

**NIST**

**National Institute of Standards and Technology**  
Technology Administration, U.S. Department of Commerce

# EFFECTS OF SPECTRAL UV ON DEGRADATION OF ACRYLIC-URETHANE COATINGS

Tinh Nguyen, Jonathan W. Martin, Eric Byrd, and Edward Embree

National Institute of Standards and Technology, Gaithersburg, MD 20899

## INTRODUCTION

Polyurethanes (PU) based on acrylic polyols are used extensively as exterior coatings. However, these materials undergo degradation during exposure to outdoor environments (1, 2). Although temperature, moisture, and other weathering elements may contribute to the degradation of polymer coatings, the primary cause of PU degradation during outdoor exposure is ultraviolet (UV) light. For that reason, the photodegradation mechanism of PU and its model compounds have been studied extensively (3-5). Both aromatic and aliphatic isocyanate-based polyurethanes undergo chain scission by photo-oxidation process. It is well known that photodegradation (photolysis and photo-oxidation) of a material is determined by the absorption characteristics of radiation in that material. However, the absorption of radiation energy in polymers is controlled by their chemical structure and is dependent on radiation wavelength. Studies on wavelength sensitivities of a variety of polymers have been reviewed (6-8). However, little information is available on the photodegradation behavior of PU with respect to radiation wavelengths (9). The main objective of the present study is to investigate the effects of different radiation wavelengths from 290 nm to 525 nm on the degradation mechanism and quantum efficiency of acrylic polyol-based polyurethanes.

Information on the mechanism is based on Fourier infrared spectroscopy analysis in the transmission mode, which measures chemical changes of the entire film thickness. The quantum efficiency at different wavelengths is estimated by:

$$\phi(\lambda) = D_{\text{dam}}(\lambda, t) / D_{\text{dos}}(\lambda, t)$$

where

$\phi(\lambda)$  : apparent quantum efficiency within the exposed radiation wavelengths, in  $\text{Am}^{-1}\text{J}^{-1}$  (A is the infrared absorbance),

$D_{\text{dam}}$  : damage, in infrared absorbance (A) units.

$D_{\text{dos}}(\lambda, t)$  : total dosage absorbed in the material, in J.

The total absorbed dosage is the total number of quanta absorbed by a material and is given by

$$D_{\text{dos}}(t) = \int_0^t \int_{\lambda_{\text{min}}}^{\lambda_{\text{max}}} E_o(\lambda) (1 - 10^{-A(\lambda)}) d\lambda dt$$

where

- $\lambda_{\min}$  and  $\lambda_{\max}$  : minimum and maximum photolytically effective UV-visible wavelengths, in nm,  
 $A(\lambda,t)$  : absorbance of sample at specified UV wavelength and at time  $t$ , (dimensionless),  
 $E_o(\lambda,t)$  : incident spectral UV-visible radiation dose on sample surface at time  $t$ , in  $\text{J cm}^{-2}$ ,  
 $t$  : exposure time, in s.

The total absorbed dosage was obtained by integrating the product of the spectral irradiance,  $E_o(\lambda,t)$ , and the spectral absorption of the coating,  $(1-10^{-A(\lambda,t)})$ , over the wavelengths of radiation impinging on the specimen for the exposure duration at a particular humidity and temperature. Both quantities were measured using UV-visible spectroscopy, while the damage was measured with FTIR. The quantum efficiency determined in this study is considered as an "apparent" value and is expressed as the change in FTIR intensity per unit thickness per amount of radiation absorbed in the coatings. If FTIR intensity of the degradation is expressed in absorbance units (A), thickness in meters (m), and absorbed radiation dosage in Joules (J), the apparent quantum efficiency is expressed in  $\text{A m}^{-1} \text{J}^{-1}$ . Since both the absorbed dosage and material damage were measured on exposed specimens, the quantum efficiency does account for the effects of relative humidity, temperature, and radiant flux on the degradation.

## Experimental Procedures

### *Material*

A model thermoset acrylic-urethane coating consisting of a mixture of a hydroxy-terminated acrylic resin and an aliphatic isocyanate cross-linking agent was used. The acrylic resin contained, by mass, 68 % butylmethacrylate, 30 % hydroxy-ethylacrylate, and 2 % acrylic acid. The isocyanate was a conventional biuret hexamethylene diisocyanate. The urethane was formulated at an OH - NCO ratio of 1, without catalyst and without light-stabilized additive. Coatings were applied to calcium fluoride ( $\text{CaF}_2$ ) substrate by spin coating followed by curing at  $130^\circ\text{C}$  for 20 minutes. All coated samples were well cured, which was evidenced from Fourier transform infrared spectroscopy (FTIR) analysis of the NCO band at  $2272 \text{ cm}^{-1}$ .  $\text{CaF}_2$  is transparent in the wavelength range between  $0.13 \mu\text{m}$  and  $11.5 \mu\text{m}$  and has excellent moisture and heat resistance. Therefore, it was possible to expose clear coated  $\text{CaF}_2$  to wide ranges of temperature, humidity, and UV radiation, while monitoring the spectral absorption and degradation of the coating by UV-visible spectroscopy and FTIR spectroscopy. The coating thickness was  $8 \mu\text{m} \pm 1 \mu\text{m}$ .

### *Instrumentation and Exposure Cells*

Figure 1 schematically shows the main components of the experimental setup used in this study. It consists of two solar simulators (the light source), an exposure cell platform, a controlling system, and instruments to measure spectral radiation energy and coating degradation. Each solar simulator's optical system is comprised of a 1000 W xenon arc lamp, a dichroic mirror, an

optical integrator, and a Fresnel collimating lens. The dichroic mirror removes the infrared portions of the xenon arc spectrum; therefore, the thermal effect induced by the radiation on the specimens was less than 2 °C above ambient temperature. The integrator homogenizes the beam while the Fresnel lens collimates the beam.

The exposure cells were designed to simultaneously expose different sections of the same film to 12 well-defined, spectral UV-visible conditions at the same temperature and relative humidity (RH). Figure 2a depicts the arrangement of the exposure cells underneath the solar simulators, and Figure 2b shows a cross section of the exposure cell. Each exposure cell has a layered design and included a filter disk, a quartz disk, a CaF<sub>2</sub> specimen disk, and an encasement to hold the disks. The filter disk contained 11 windows--10 on the disk perimeter and the eleventh in its center. Each window was 16 mm in diameter. Each of the 10-perimeter windows was outfitted with a band pass filter covering a different segment of xenon arc spectral spectrum from 290 nm to 525 nm. The center window was outfitted with a 300 nm cut-on filter (allowed only wavelengths >300 nm to be transmitted). The broadness of each wavelength range and the transmission of the 10 band pass filters are given in Figure 3. The first eight filters had full-width-half-maximum (FWHM) values between 2 nm and 10 nm and covered the range between 290 nm and 340 nm.

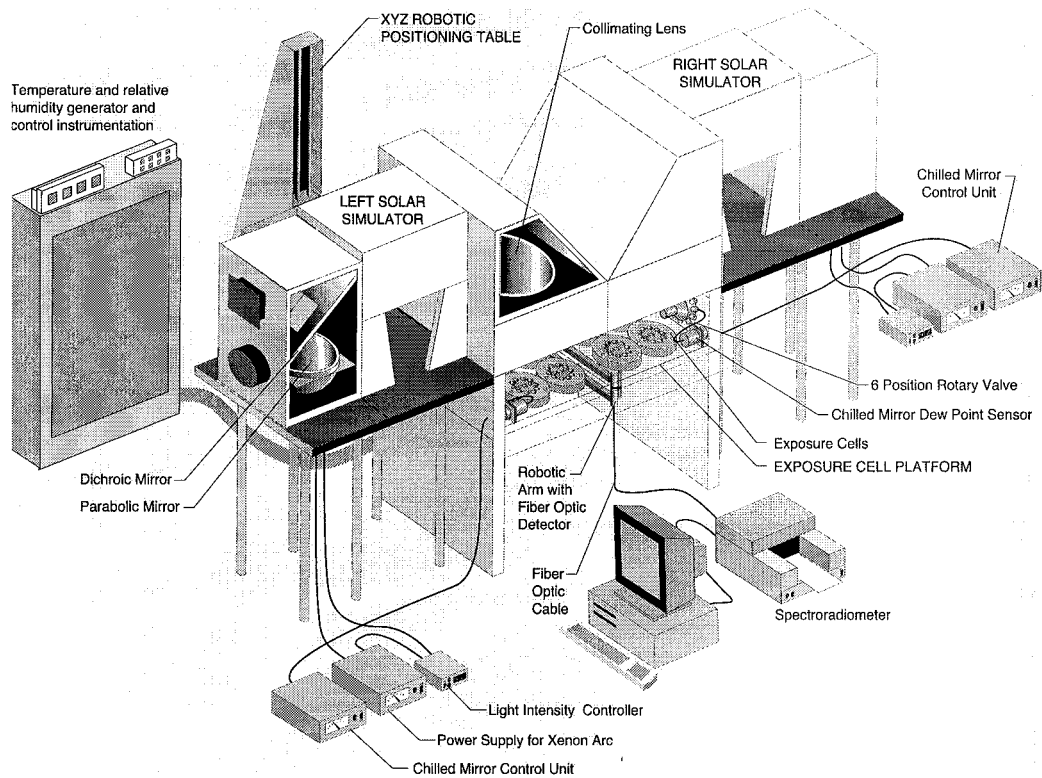
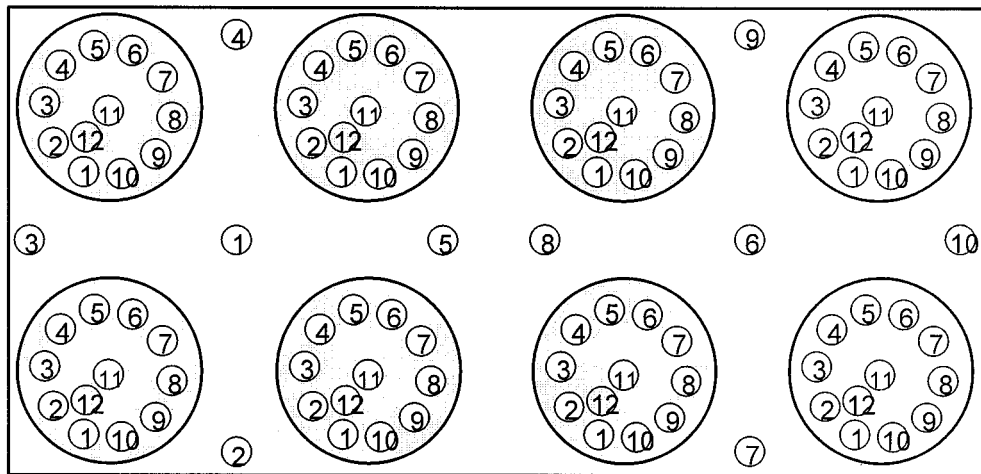
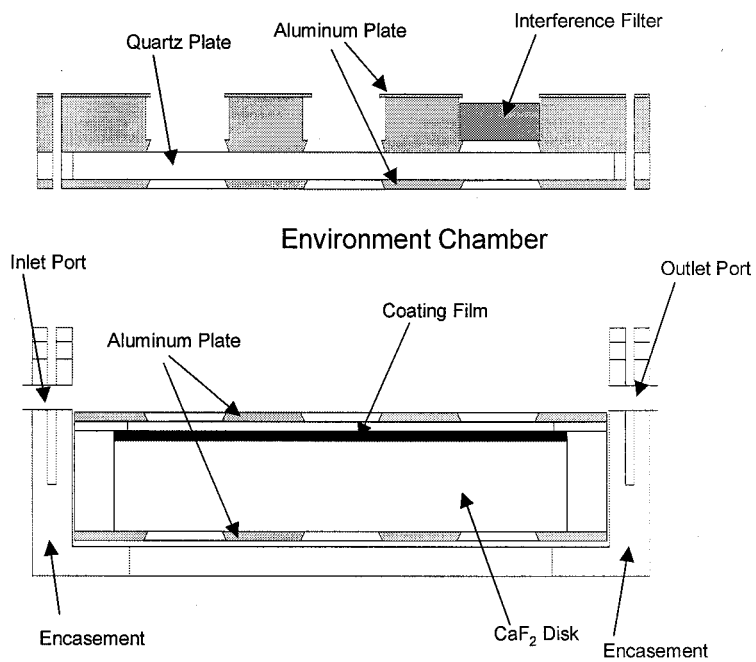


Figure 1. Experimental setup for measuring absorbed dosage and quantum efficiency of coatings exposed to different spectral UV/relative humidity/temperature conditions.



**a**



**b**

Figure 2. a) Arrangement of exposure cells, and b) cross section of an exposure cell.

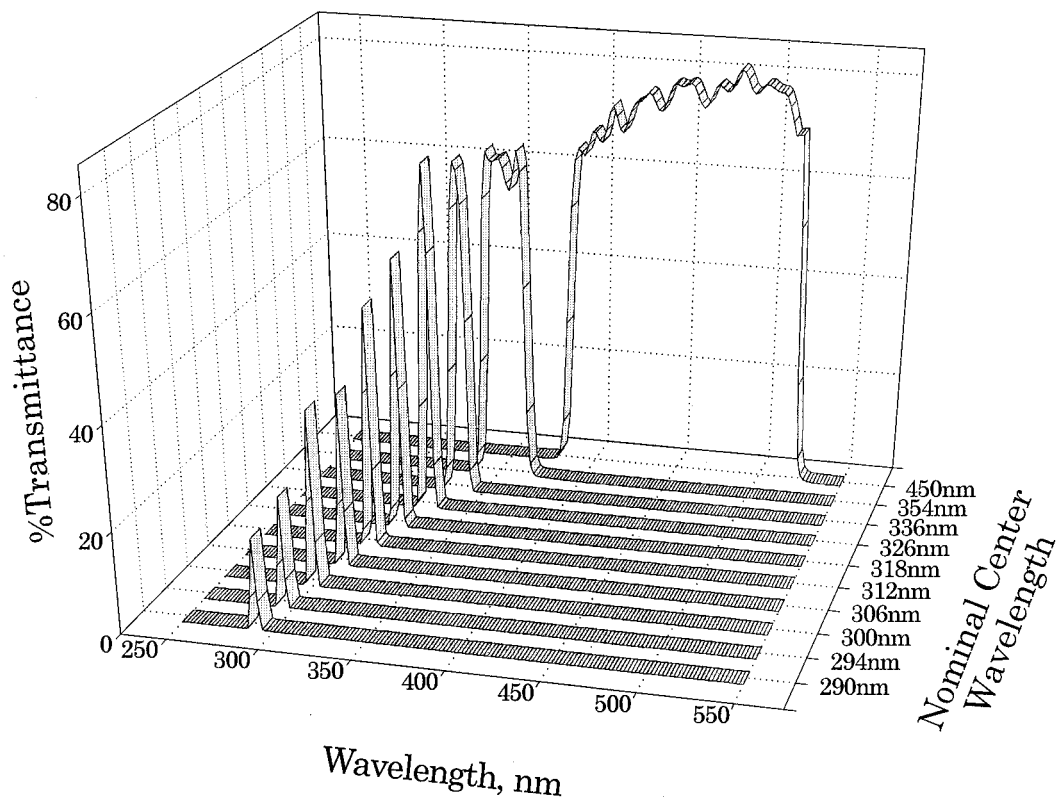


Figure 3. Characteristics of the 10 band-pass filters used to provide different spectral UV ranges.

The nominal center wavelengths for these filters were 290 nm, 294 nm, 300 nm, 306 nm, 312 nm, 318 nm, 326 nm, and 336 nm. The two remaining filters had FWHM values greater than 10 nm and had center wavelengths of 354 nm and 450 nm. Hereafter, the band pass filters are also referred to by their center wavelengths, e.g., 290 nm filter, 354 nm filter, etc. In addition, changes in specimens that was exposed in the absence of UV light (no-UV) (no. 12 in Figure 2a) were also measured to assess non-photolytically induced degradation.

The space between the quartz disk and coated  $\text{CaF}_2$  disk served as the environmental exposure chamber. The exposure cell was machined to tight tolerances so that a positive pressure could be maintained within the exposure chamber of an exposure cell. Inlet and outlet ports were drilled into the exposure cell to circulate the desired temperature/RH condition into the chamber. The conditioned air was generated in a humidity-temperature generator and pumped into each exposure cell. The humidity generators were fabricated based on the principle of dry/moisture-saturated air mixture. The temperature within the exposure chamber was monitored via a thermocouple and RH was monitored by a chilled mirror hygrometer. The RH at a specified temperature in each cell was tracked by a feedback-control system, which monitored both the temperature and RH within the exposure cell three times per second. The temperature and RH could be maintained within 0.5 % and 3 %, respectively, of their set values.

### *Measurements of Absorbed Dosage and Coating Degradation*

To accurately estimate the total dosage absorbed in the film, the optical properties of all of the components must be measured, including 1) the spatial and spectral variability in the radiant flux of the light source, and 2) spectral transmittances of the band pass filters, quartz disks, and coated CaF<sub>2</sub> disks for all eight exposure cells. Spatial and temporal changes of lamp intensity were monitored using an UV-visible spectrometer connected to a robotic controlling system via a fiber optic cable. These measurements were done in the absence of the exposure cells. Measurements of the optical properties of the system components were highly automated by the use of a robotic arm and an automated sampler. The robotic-controlled fiber optic cable probe had the capability of moving in the X, Y, and Z directions, and the spectrometer was programmed to make measurements at frequent time intervals at 98 different locations on the platform table (88 corresponding to 11 filters on each of the eight exposure cells and 10 locations outside the exposure cells).

UV absorption in the coatings was obtained from the transmission of light passed through the band pass filters, the quartz plate, and the coated CaF<sub>2</sub> plate. At each specified time interval, the coated CaF<sub>2</sub>-contained exposure cell was removed from the platform table and fitted into a demountable 150-mm diameter ring of an auto-sampling accessory. The ring was computer-controlled and can be programmed to rotate and translate over the entire sampling area. Spring-loaded Delrin clips ensure that the specimens are precisely located and correctly registered. The auto-sampler was placed in the UV spectrometer compartment and UV-visible spectra were taken at 2 s per scan using a customized computer program. This automated sampling system allowed unattended, efficient, and quick recording of the UV transmission of the coating at all 12 windows of an exposure cell. Since the exposure cell was mounted precisely on the auto-sampler, error due to variation of sampling at different exposure times was essentially eliminated. Transmission measurements were also taken individually for the quartz, the coated CaF<sub>2</sub>, and the bare (uncoated) CaF<sub>2</sub> plates. To improve the accuracy of these measurements, the UV-visible spectrometer was calibrated during each inspection against standard UV-visible spectrometer transmittance density filters using NIST Standard Reference Material (SRM 930d). From the amount of light transmitted through each component of the exposure cell as a function of time, the light intensity impinging upon, as well as absorbed by, the coatings was determined. Both of these quantities are required inputs for estimating the absorbed dosage and quantum efficiency.

Damage in the coating was measured by transmission FTIR spectroscopy. FTIR spectra were taken using the same auto-sampler described above placed in an FTIR spectrometer equipped with a liquid nitrogen-cooled mercury cadmium telluride (MCT) detector. All FTIR spectra were the average of 132 scans recorded at a resolution of 4 cm<sup>-1</sup> using dry air as the purge gas. The peak height method was used to represent IR intensity, which is expressed in absorbance, A. The FTIR spectrometer was calibrated against a polystyrene film during each inspection. All results were the average of three specimens. A software program was written to estimate total absorbed dosage, material damage, and quantum efficiency.

## Results and Discussion

### *Spatial Uniformity and Temporal Stability of UV Light Source*

Results on spatial uniformity, collimation and temporal stability of the UV light source have been given elsewhere (9). In general, the spectral radiant flux of the xenon arc light sources changed with time. The magnitude of the changes differed from one wavelength to another. For example, after 1500 h of operation, the spectral radiant flux decreased, with respect to initial values, at 290 nm, 326 nm, and 450 nm by 25 %, 50 %, and 38 %, respectively. These changes demonstrate the need for frequent monitoring of the spectral radiant flux of the light source. The radiant flux also differed from one solar simulator to another and varied from one lamp to another. Moreover, the spatial variation in the radiant flux over the working plane of both simulators was high. This high spatial variability in the irradiance pattern necessitates a large number of measurements to characterize the spatial variation.

Beam collimation and scattering of the radiation were ascertained by measuring the radiant flux at the center points of several randomly selected windows. Measurements started at a point immediately below the exposure cell window and, then, at 10 mm increments below this point until the sensor was 100 mm vertically beneath its initial position. Radiant flux measurements were plotted against vertical distance and regression analysis was performed. The slope of the regression curve was not significantly different from zero suggesting that the radiant output from each solar simulator was highly collimated. The absence of stray light incident on the covered 12<sup>th</sup> window was verified by positioning the fiber optic probe immediately beneath this window; no UV-visible radiation was detected. The band pass filters were photolytically and thermally stable, except for the 450 nm filters, which lost 2 % to 7 % of their transmittance after over 1000 h exposure. The CaF<sub>2</sub> did not exhibit any transmittance change and the quartz plates showed a small transmission loss over the course of exposure. All of these changes were accounted for in the calculation of absorbed dosage.

### *Coating Degradation*

Examples of FTIR results on coating degradation are given in this section to demonstrate the approach for measuring the material damage and calculating the spectral quantum efficiency in the samples. Figure 4 presents typical FTIR spectra of the coating before and after aging for two different times under the 300 nm cut-on filter (KG) at 50 °C/~0 % RH condition. The major FTIR bands of interest in a cured, unaged acrylic-urethane coating based on an acrylic polyol and an aliphatic isocyanate are the bands at 3380 cm<sup>-1</sup>, due to NH stretching, 1730 cm<sup>-1</sup>, due to C=O stretching of the urethane linkage, 1520 cm<sup>-1</sup>, due to amide II (NH bending and CN stretching), and 1250 cm<sup>-1</sup>, due to amide III (NH bending and CN stretching). The assignments are based on extensive IR data of polyurethanes (11).

Although a comparison between spectra of the unaged and aged samples, as shown in Figure 4, can give some information about the effects of exposure on a polymer film, the degradation behavior is best studied from the difference spectra, where the formation or depletion of a band and the appearance of a new species can be readily observed. Examples for such difference spectra as a function of spectral UV ranges and exposure times for samples exposed under the

cut-on filter (KG) in 50 °C/~0%RH condition are displayed in Figures 5a and 5b, respectively. The bands above and below the zero line in a difference spectrum indicate a gain and loss, respectively, of chemical species in the film.

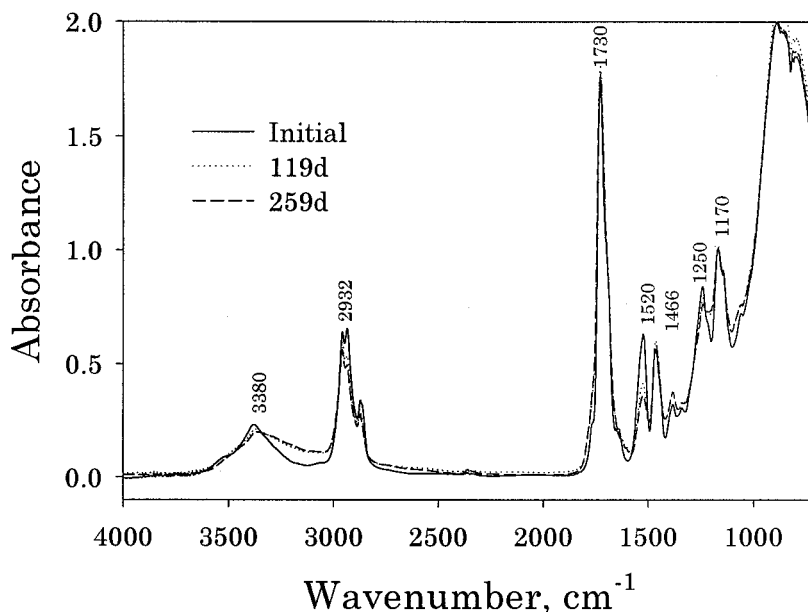


Figure 4. Typical FTIR spectra of PU coating before and after exposures for two different time intervals under the 300 nm cut-on filter in 50 °C/~0% relative humidity condition.

The degradation observed at 50 °C/dry condition in the absence of radiation (no-UV) was small compared to that of other UV light ranges. Various compounds were formed during exposure to UV, as evidenced by the appearance of the bands at 1752 cm<sup>-1</sup>, 1418 cm<sup>-1</sup>, and in the 3100 cm<sup>-1</sup> to 3300 cm<sup>-1</sup> region. Similarly, the intensity of the bands at 1730 cm<sup>-1</sup>, 1520 cm<sup>-1</sup>, 1250 cm<sup>-1</sup> and in the CH region between 2800 cm<sup>-1</sup> to 3100 cm<sup>-1</sup> decreased markedly with exposure times. These results indicate that the PU material has degraded substantially after more than eight months of exposure. Further, all the bands that were formed occurred at the same positions irrespectively of the wavelength ranges studied. The same band positions in the IR spectra indicate that the same chemical groups were produced during the photodegradation at different wavelengths. This result suggests that, despite a substantial variation in the extent of degradation among the UV wavelength ranges, essentially no effect of wavelengths on the primary photodegradation mechanism of this polyurethane material was observed. Such wavelength insensitivity implies that the degradation in this material was induced by chromophores initially present in the films.

The C=O band at 1752 cm<sup>-1</sup> (of acetyl urethane, O=C-NH-C=O ) and the NH band at 1520 cm<sup>-1</sup> were used to follow the oxidation and chain scission, respectively. Figures 6a and 6b depict FTIR intensity changes of these two bands as a function of time for the cut-on filter and 10 center wavelengths. In these figures, each symbol represents a data point, which was the average

of three specimens, as stated in the experimental section. The coefficients of variation for all data points were  $<7\%$ , indicating that the reproducibility of the results between the specimens was good. As can be seen in these figures, there is no particular order for both the rate and magnitude of degradation with regards to wavelength, despite the fact that the shorter wavelengths contain higher-energy photons. However, the 294 nm and 300 nm filters appeared to cause the least damage. This was true for both oxidation and chain scission. The oxidation for all wavelength ranges was greater at earlier time then became almost constant at prolonged exposure. For chain scission, the degradation was fast during the first 50 days but slowed down thereafter.

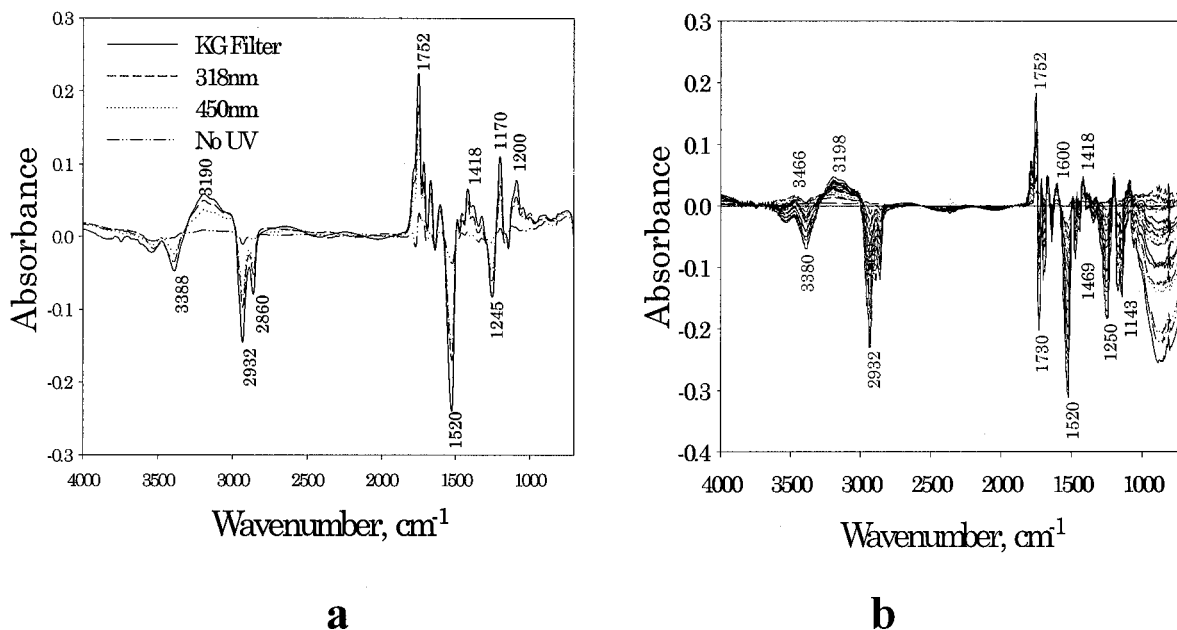


Figure 5. Difference spectra of PU exposed for: a) 180 d under no UV and several spectral UV ranges, and b) for different times under the 300 nm cut-on filter, in  $50\text{ }^{\circ}\text{C}/\sim 0\%$  RH condition.

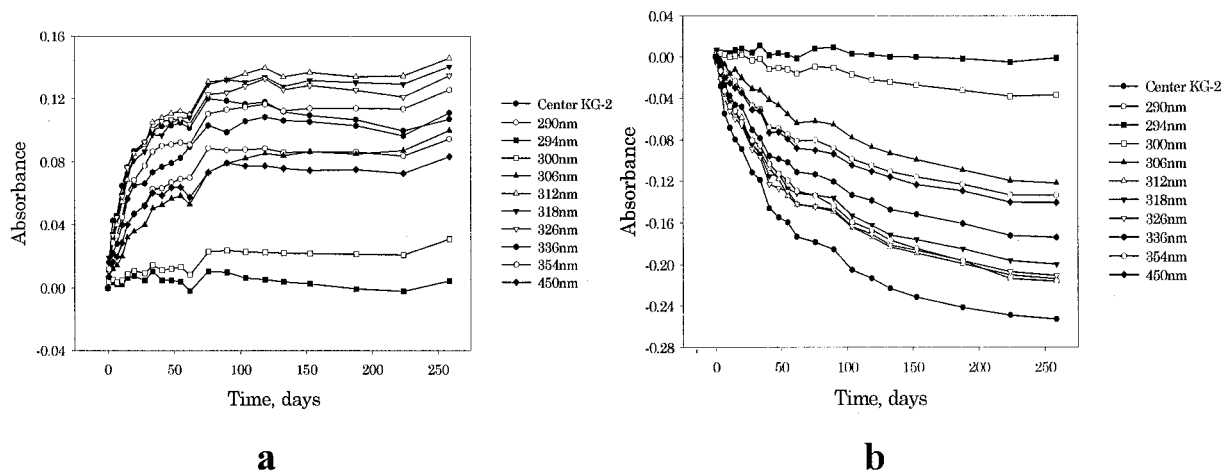


Figure 6. FTIR intensity changes of PU with exposure time in  $50\text{ }^{\circ}\text{C}/\sim 0\%$  RH for the 300 nm cut-on filter (KG) and 10 different center wavelengths; a) oxidation, and b) chain scission.

## Total Absorbed Dosage and Apparent Quantum Efficiency

Photons of lower wavelength radiation are more energetic than those of higher wavelengths, and far fewer photons of the lower wavelength radiation actually impinged upon the sample surface. Therefore, the damage/time relationship as shown in Figure 6 is not valid for comparing the effects of different wavelengths on polymer degradation. The relative effects may be observed in the damage/absorbed dosage plot because only radiation absorbed in the material that causes degradation is really taken into account. Figures 7a and 7b display photo-oxidation and chain scission, respectively, as a function of absorbed dosage for specimens exposed to cut-on filter (inset) and 10 band pass filters under 50 °C/~0 %RH condition.

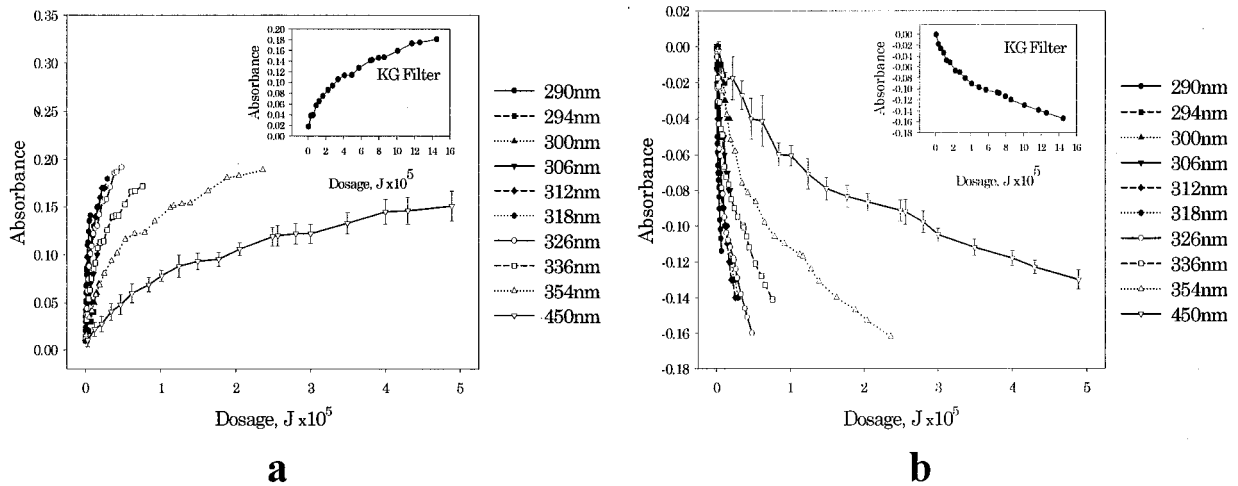


Figure 7. FTIR intensity change with absorbed dosage for PU exposed to 50 °C/~ 0%RH condition for one cut-on filter (KG) and 10 different center wavelengths; a) oxidation, b) chain scission.

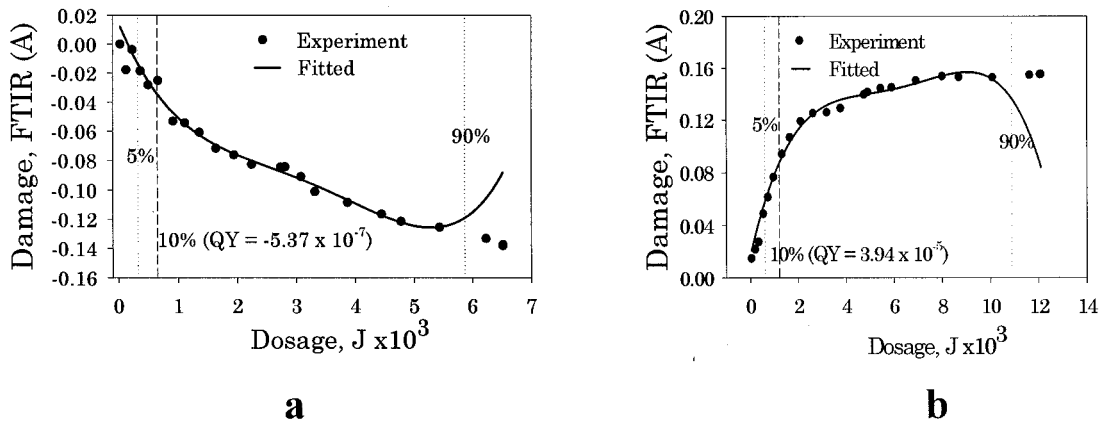


Figure 8. Experimental and fitting FTIR degradation data as a function of absorbed dosage for a) chain scission, and b) oxidation. The initial slopes of these curves are used for obtaining the quantum efficiency.

It should be noted that only data involved in the photolytic process are included in Figure 7. That is, the results measured in the absence of UV light at the same temperature and RH were removed from the total degradation. The absorbed dosage, i.e., the actual amount of radiation absorbed by the coating, was calculated using the equation given above. All dosages were measured after 250 d of exposure. As expected, samples under the cut-on filter (KG) and long wavelength band pass filters absorbed the most dosage while those exposed to short wavelengths absorbed less. Further, radiation from the lower wavelength filters caused more rapid degradation than higher wavelengths, as evidenced by the slopes of the curves.

The apparent quantum efficiency was taken as the initial slope of the damage/total absorbed dosage curve. The use of this initial slope avoids complications from multiple degradation processes and from potential shielding of the coating material by degradation products absorbing radiation. In the process of determining this slope, a fourth-order polynomial function was fitted to the damage/total absorbed dosage curve. In this first implementation of analyzing this curve, the slope at the 10 % of the total absorbed dosage was used as the end point. One example of such fitting is shown in Figure 8 for the chain scission process ( $1520\text{ cm}^{-1}$  band) and oxidation ( $1752\text{ cm}^{-1}$  band) of samples under the 450 nm filter. In this figure, the symbols are the experimental data and the solid lines are the fitted curves. The initial part of the damage/absorbed dosage curves at  $1520\text{ cm}^{-1}$  exhibits some scatter due to imprecision in the measurements of very small changes at early exposures. Nevertheless, the polynomial function fit most of the data well. Differentiating the polynomial gives the slope (apparent quantum efficiency) at a given absorbed dosage. Since the damage/absorbed dosage relationship is not linear, the apparent quantum efficiency falls off with total absorbed dosage, presumably due to increasing shielding of the coating by degradation products and to the depletion of weak links in the material. Note that the negative values in Figure 8a vertical axis are indicative of a loss of material.

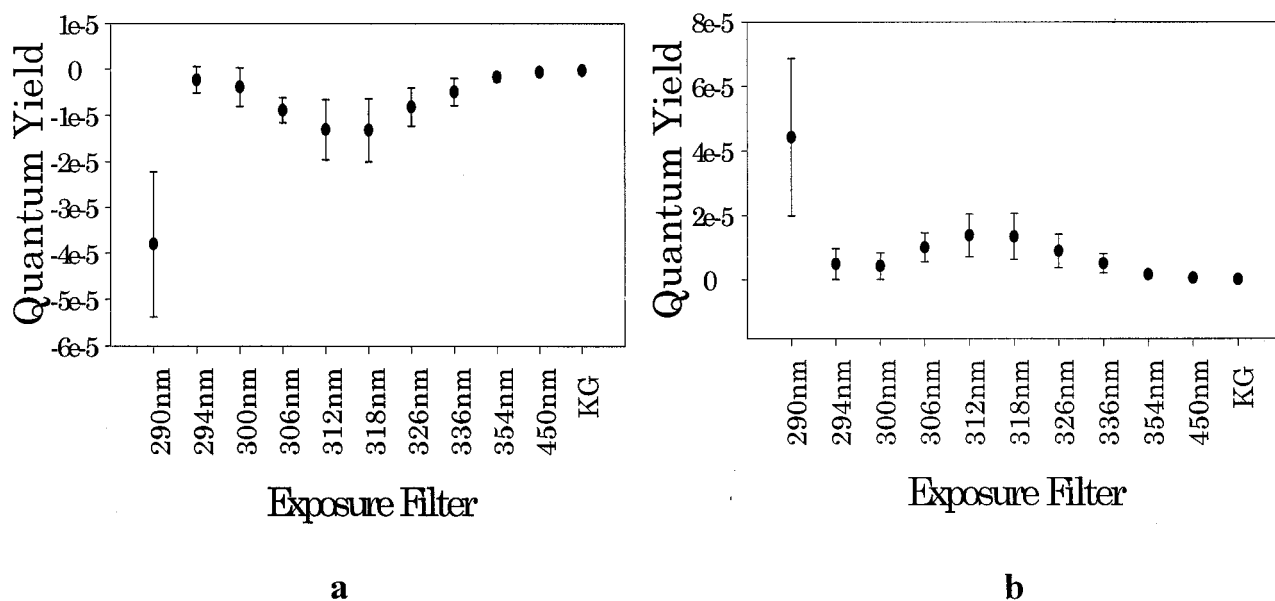


Figure 9. Quantum efficiency of a) chain scission and b) oxidation of an acrylic-urethane coating exposed to  $50\text{ }^{\circ}\text{C}/\sim 0\text{ \% RH}$  for 300 nm cut-on filter and 10 different center wavelengths.

Figure 9 presents apparent spectral quantum efficiency for the oxidation and chain scission of PU coating exposed to 50 °C/~0 %RH for a cut-on filter (KG) and ten different center wavelengths. The one-standard error bars are included in the curves. The quantum efficiency at 290 nm appears to be the highest. Although the samples under the cut-on filter and long center wavelengths, i.e., 450 nm and 354 nm filters, absorbed the most energy, their quantum efficiency was similar to other filters. Since the unit employed to express quantum efficiency in this study is different from that traditionally used (number of molecules that undergo change/number of quanta absorbed), it is difficult to compare directly the values obtained here with data reported for polymers reported in the literature. Work is in progress to measure the molar absorption coefficients of the infrared bands of interest, and the results will be used to convert IR absorbance units into number of molecules. Nevertheless, the quantum efficiencies in all spectral UV ranges for this PU were small, as is typical for solid polymers. For example, the quantum yield of hydroxyl formation in polyurethanes exposed to 315 nm and 365 nm radiation has been reported to be  $0.002 \pm 0.001$  and  $0.005 \pm 0.001$ , respectively (number of OH formed/number of quanta absorbed) (9). Quantum yields of chain scission for other polymers also range between  $10^{-2}$  to  $10^{-5}$  (12). It should be mentioned that the quantum yield of polymer chain scission changes rapidly from below to above the glass transition temperature (T<sub>g</sub>). Further, above T<sub>g</sub>, the quantum yield is similar to that irradiated in solution, which is several order of magnitude greater than that in solid (12). Thus, photodegradation of PU materials is expected to be more rapid if they are used at temperatures higher than their T<sub>g</sub>.

## Summary and Conclusions

Polyurethanes are used extensively as exterior coatings. However, these materials undergo degradation during outdoor exposure. The effects of spectral UV on photodegradation mechanism and quantum efficiency of an acrylic-urethane coating was investigated. Damage was measured by transmission Fourier transform infrared spectroscopy, and radiation energy absorbed in the sample for each wavelength range was estimated from measurements of spectral irradiance and spectral absorption of the coating using UV-visible spectroscopy. Ten spectral wavelength ranges covering from 290 nm to 525 nm were generated using band pass filters, which allow certain radiation wavelengths passing through and interact with the samples. Samples exposed in the absence of UV and under 300 nm cut-on filters were also analyzed. The UV light source was provided by two 1000 W xenon arc lamps, which contained radiation from 270 nm to 800 nm. Samples were prepared by applying a mixture of an acrylic polyol with an aliphatic triisocyanate to calcium fluoride substrates. They were exposed to 50 °C and ~ 0 % relative humidity for more than eight months. FTIR results showed that the degradation mechanism of PU was essentially the same regardless of the center wavelengths from 290 nm to 450 nm. Both the rate and extent of the photodegradation with respect to absorbed dosage varied with wavelength. However, except for the 290 nm filter, which appeared to have the highest value, the quantum efficiency of other wavelength ranges did not differ greatly. Knowledge of the spectral quantum efficiency in the UV-visible region is essential for developing improved photo-accelerated tests and more photo-stable materials.

## References

- 1) Bauer, D., J. Gerlock, D. Mielewski, M.C. Peck, and R.O. Carter (1991), 'Photodegradation and photostabilization of urethane cross-linked coatings,' *Ind. Eng. Chem. Res.*, 30 (11), 2482-2487.
- 2) Wernstahl, K.M. (1996), 'Service life prediction of automotive coatings, correlating infrared measurements and gloss retention,' *Polymer Degradation and Stability*, 54, 57-65.
- 3) Wilhelm, C. and J.L. Gardette (1997), 'Infrared analysis of the photochemical behavior of segmented polyurethanes: 1. Aliphatic poly(ester-urethane),' *Polymer Degradation and Stability*, 38, 4019-4031.
- 4) Wilhelm, C. and J.L Gardette (1998), 'Infrared analysis of the photochemical behavior of segmented polyurethanes: 3. Aromatic diisocyanate based polymers,' *Polymer Degradation and Stability*, 39, 1223-1232.
- 5) Rabeck, J. F. (1995), *Polymer Photodegradation, Mechanism and Experimental Methods*, Chapman & Hall, pp 308-316, and references therein.
- 6) Searle, N.D. (1986), 'Wavelength sensitivity of polymers', in *Advances in the Stabilization and Controlled Degradation of Polymers*, A. V. Patsis, ed. Technomic Publishing, Landcaster, pp 62-74.
- 7) Trubiroha, P. (1986), 'The spectral sensitivity of Polymers in the spectral range of solar radiation,' in *Advances in the Stabilization and Controlled Degradation of Polymers*, A. V. Patsis, ed. Technomic Publishing, Landcaster, pp 236-241.
- 8) Andrady, A.L. (1997), 'Wavelength sensitivity in polymer photodegradation' in *Advances in Polymer Science*, 128, Springer, New York, pp 47-94.
- 9) Gardette, J.L. and J. Lemaire (1984), 'Photothermal oxidation of thermoplastic polyurethane elastomers: Part 3 - Influence of the excitation wavelengths on the oxidative evolution of polyurethanes in the solid state,' *Polymer Degradation and Stability*, 6, 135-148.
- 10) Martin, J.W., T. Nguyen, E. Byrd, N. Embree, and B. Dickens (2002), 'Relating laboratory and outdoor exposures of coatings: I. Cumulative damage model and laboratory exposure apparatus,' *Polymer Degradation and Stabilization*, 75, 193-210.
- 11) Srichatrapimuk, V.W. and S. Cooper (1978), 'Infrared thermal analysis of polyurethane block polymers', *J. Macromol. Sci., Phys.*, B15 (2) 267-311.
- 12) Randy, B. and J.F Rabeck (1975), *Photodegradation, Photo-oxidation and Photostabilization of Polymers: Principles and Applications*, John Wiley & Sons, New York, pp 83-87.